DESIGN AND RESEARCH OF MEDICAL HIGH VOLTAGE POWER SUPPLY BASED ON NONLINEAR ADAPTIVE PID CONTROL

Yao CHEN[1], Yajun WANG[2,*], Yujun YU[3]

The traditional high-voltage (HV) power supply with PID control algorithm has large output ripple and poor output voltage stability. A single neuron adaptive PID control based HV power supply for medical mammography X-ray machine is designed in this paper. Since the neural network has self-learning function, self-adaptability and non-linear function representation capability, the PID parameters can be adjusted online to realize accurate tracking and control. The test results show that the designed HV power has small output voltage ripple, high robustness, small overshoot, which can be applied to medical mammography X-ray machine and other medical high voltage equipment.

Keywords: HV power supply; medical mammography X-ray machine; single neuron adaptive PID; nonlinear system; bi-directional voltage doubling circuit

1. Introduction

At present, various kinds of X-ray machines are widely used in medical equipment. X-ray tube is the core device of the system. In practical application, since the penetration of X-ray is closely related to the tube voltage, the ray intensity will increase with the increase of the tube voltage. Therefore, the performance of high-voltage power supply is the key factor to determine the performance of the whole equipment.

The traditional high-voltage power supply is mostly controlled by PID control algorithm. PID control, as the representative of classical control theory, is simple in structure and easy to implement. However, the control parameters are difficult to adjust automatically with the changes of environment and are vulnerable to interference. Meanwhile, it is difficult to meet the requirements of stability and robustness of high-voltage power supply. Chen et al [1] and Xiao [2] proposed a self-tuning fuzzy PID control algorithm, which improves the response

[1] Postgraduate, School of Electronic and Information Engineering, Liaoning University of Technology, Jinzhou, Liaoning, China
[2] Prof., School of Electronic and Information Engineering, Liaoning University of Technology Jinzhou, Liaoning, China
[3] Postgraduate, School of Electronic and Information Engineering, Liaoning University of Technology, Jinzhou, Liaoning, China
* Corresponding author: Yajun Wang, email: wyj_lg@163.com

speed. However, the fuzzy control rules need to be determined by experts' experience and rely on prior knowledge. Qu and Hao [3] proposed a variable parameter quadratic performance optimization PID control algorithm with the ability of anti-integral convergence, which has high stability and robustness, but the structure is complex and difficult to realize. Bhatti et al [4] and Yu et al [5] presented a neural network control method. Although the parameters of the controller can be adjusted online, the amount of data calculation is huge. Tao et al [6] developed a nonlinear control strategy for dynamic system identification. The method is aimed at nonlinear control objects. Qiang et al [7] proposed a resonant soft switching inverter with auxiliary commutation, which realized zero voltage switching operation of switching devices. Chen et al [8] presented a high voltage power converter for TWT amplifier, which has good soft switching characteristics.

This paper aims at the research of high-voltage power supply for medical mammography X-ray machine. According to the requirement, the output voltage is designed to be 30KV. Since the mammography X-ray machine requires high working environment [9], and high voltage power supply is a nonlinear system with AC-DC conversion. Traditional PID control is difficult to meet the requirements. Hence, nonlinear control system is designed to control the medical high voltage power supply. Since neuron control method has strong adaptive ability [10] and good nonlinear resolution ability, single neuron control and traditional PID controller are combined to solve the nonlinear problem of high voltage power supply by using the ability of nonlinear control to have good approximation characteristics to nonlinear objects. Simultaneously, through online adjustment of its own weight value, the optimal value can be found to adjust the parameters of PID controller to adapt to the changes of parameters, structure and input signals of the controlled system and resist the influence of external disturbance. Therefore, single neuron adaptive PID nonlinear control algorithm is proposed in this design. The experimental results show that the high-voltage power supply for X-ray tube designed in this paper can output a voltage of 30KV with a ripple of ±2.6%. Compared with the traditional PID algorithm, the proposed method has high robustness, small overshoot and fast response, which meets the design requirements.

2. Overall design scheme

X-ray tube power supply voltage is generally tens of thousands of volts to hundreds of thousands of volts. The traditional linear power supply has large calorific value, low efficiency, general performance and large volume. However, with the development of switching power supply technology, switching power supply is commonly used in DC regulated power supply with high precision and

high voltage stabilization requirements, low ripple and large voltage difference due to its high efficiency [11]. Therefore, switching power supply technology is used to supply power to the X-ray tube in this design.

In the past high-voltage power supply design, hard switch, half bridge inverter and traditional double voltage rectifier are used. Although the structure is simple, there are many disadvantages. In the process of opening and closing, the loss of hard switch is large, and the switch device is easy to be damaged due to overheating [12]. Hence, the soft switch technology is used in this paper to overcome the shortcomings of hard switch and reduce the switching noise.

The overall design scheme is shown in Fig. 1. The commercial power is converted into direct current through rectifying and filtering circuit, and then high frequency square wave is generated by inverting circuit, which is boosted by high-frequency step-up transformer. DC high voltage is output through voltage doubling rectification circuit. The voltage doubling circuit adopts a C-W positive and negative bidirectional five times voltage rectifying circuit. PWM pulse width modulation is selected as the control link of the closed-loop regulation. The output voltage is sampled and sent to the single neuron nonlinear adaptive PID controller to complete the PWM pulse width adjustment.

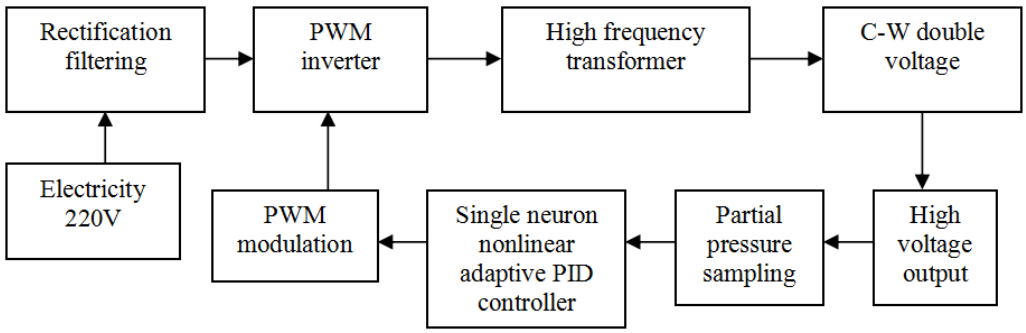

Fig. 1. The overall design scheme block diagram

3. Design of main circuit

3.1 Design of invert circuit

PWM full bridge inverter circuit is adopted as the inverter circuit, as shown in Fig. 2.

Four IGBT1~IGBT4 in the circuit are switching devices, D11~D14 are continuous current diodes, L is resonant inductor, R is equivalent resistor of resonant inductor, and T is high frequency transformer. DC 300V voltage is converted into high frequency square wave through four IGBT. In this study, the duty cycle is adjustable from 35% to 55%, and the square wave frequency is 25 kHz.

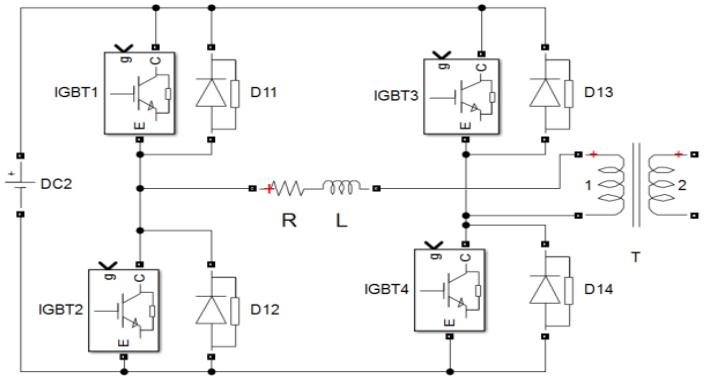

Fig. 2. The invert circuit

Since the soft switch technology can reduce the switching loss and switching noise [13,14], the working frequency of the switch device can be greatly improved. Therefore, the resonant circuit is selected to realize the soft switch technology in this design. The junction capacitor C of the switching tube performs LC resonance with the inductor L.

When IGBT1 and IGBT 4 are turned on, the power supply supplies energy to the resonant circuit and the voltage across the capacitor is

$$u_c(t) = e^{-\delta t}\sqrt{C_1^2 + C_2^2}\sin(\omega t + \varphi) + \frac{E}{1 + \frac{R}{R_L}} \tag{1}$$

When R is further greater than RL, the voltage waveform at both ends of the capacitor is in the form of sine wave through the parallel resonant circuit. Similarly, when IGBT2 and IGBT 3 are turned on, the output at both ends of resonant capacitor C is also in the form of sine wave. The switching device is turned on from zero voltage (ZVS) [15], which realizes soft switching technology.

3.2 Design of high frequency transformer

Different from the ordinary power frequency transformer, the high frequency transformer designed in this paper is in the high frequency environment of 25 kHz. Hence, the selection of the magnetic core is crucial for the transformer design. The area product method (AP) is used to select the magnetic core of the high frequency transformer [16]. When the transformer is applied to the full bridge inverter circuit, the AP expression is

$$AP = A_w A_\varepsilon = \frac{P_o\sqrt{\delta}}{\eta K J B_m f} \times 10^4 \tag{2}$$

where η is the transformer efficiency, K is the window function, J is the current density, B_m is the maximum working flux density of the magnetic core, f is the working frequency of the system power supply, δ is the duty cycle.

The expression of primary coil turns is

$$W_P = \frac{U_i t_{on}}{B_m A_\varepsilon} \times 10^4 \tag{3}$$

where U_i is the lower limit of the primary input voltage of the transformer, t_{on} is the maximum conduction time, and A_ε is the effective cross-sectional area of the selected magnetic core.

The expression of secondary coil turns is

$$W_s = \frac{W_P}{n} \tag{4}$$

where n is the ratio of primary and secondary turns, i.e. the ratio of primary input voltage to secondary voltage.

In order to reduce the high-frequency leakage inductance and the distributed capacitance of the transformer, the layered and segmented winding method can be used when winding the transformer.

3.3 Design of voltage doubling rectification circuit.

Since traditional C-W voltage doubling rectification circuit has high ripple coefficient and large internal voltage drop [17,18], a C-W positive and negative bidirectional five times voltage rectifier circuit is designed to reduce the internal voltage drop of the double voltage rectifier circuit and improve the stability and efficiency of the power supply. The special circuit is shown in Fig. 3.

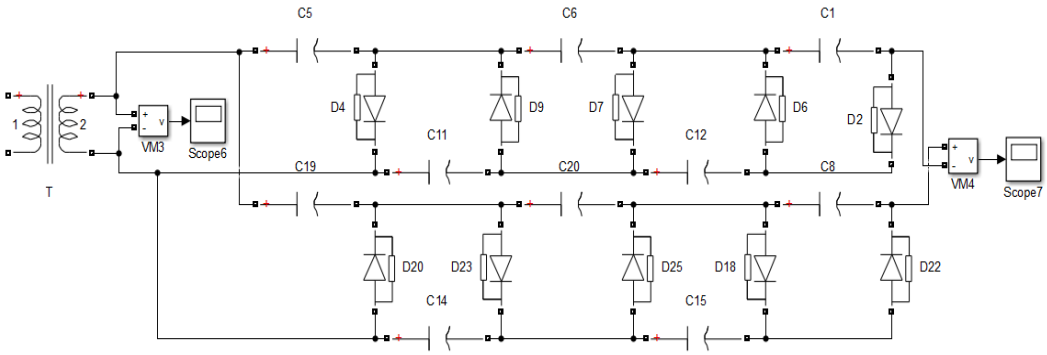

Fig. 3. Voltage doubling rectification circuit

The voltage doubling rectification circuit realizes voltage doubling and rectification of high-frequency voltage through capacitor charging and discharging and alternating conduction of diodes. In the positive half cycle of U2, C5 is charged to the peak value through D4; In the negative half cycle of U2, C11 is charged to 2U2 through C5 and D9, meanwhile C19 is charged through D20. When U2 is in the positive half cycle again, C6 is charged to 2U2 through D7, while the peak value of U2 plus the voltage of C19 charges C14, and its charging voltage can reach 2U2 through D23. Repeatedly, the final output voltage is the

sum of the absolute value of the positive and negative multiple pressure. Since the pulse coefficient is the sum of its vectors, the positive and negative pulse values cancel each other. Consequently, the ripple coefficient of the power output can be greatly reduced.

Output voltage of conventional voltage doubling rectifier circuit is calculate by

$$\Delta U = \frac{I_o}{f\mathbb{C}}\left(\frac{2}{3}n^3 + \frac{1}{2}n^2 - \frac{1}{6}n\right) \tag{5}$$

The output ripple of the conventional voltage doubling rectifier circuit is calculated as follows.

$$\delta u = \frac{I_o}{fC} \cdot \frac{n(n+1)}{4} \tag{6}$$

where n is the number of voltage doublers; I_o is the output current, and f is the switching frequency.

The output voltage of the C-W positive and negative bidirectional voltage doubling rectifier circuit is calculated by

$$\Delta U = 2 \cdot \frac{I_o}{f\mathbb{C}}\left(\frac{2}{3}n^3 + \frac{1}{2}n^2 - \frac{1}{6}n\right) \tag{7}$$

The output ripple of the C-W positive and negative bidirectional voltage doubling rectifier circuit is calculated as follows.

$$\delta u = \frac{I_o}{fC} \cdot \frac{n}{4} \tag{8}$$

The output ripple waveforms of the two voltage doubling rectifier circuits are shown in Fig. 4. As can be seen from Fig. 4, the output ripple of the conventional method is larger than the proposed method.

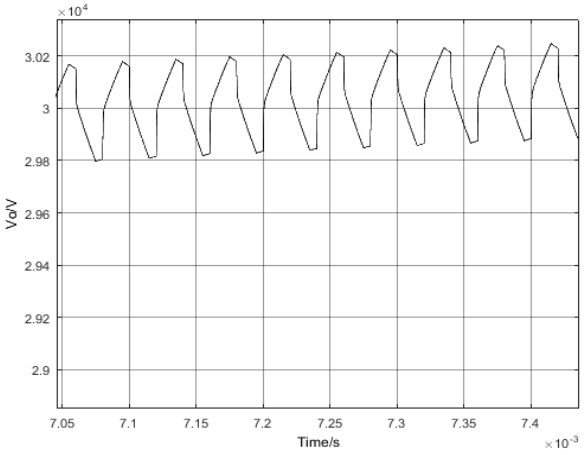

(a) Conventional voltage doubling rectifier circuit

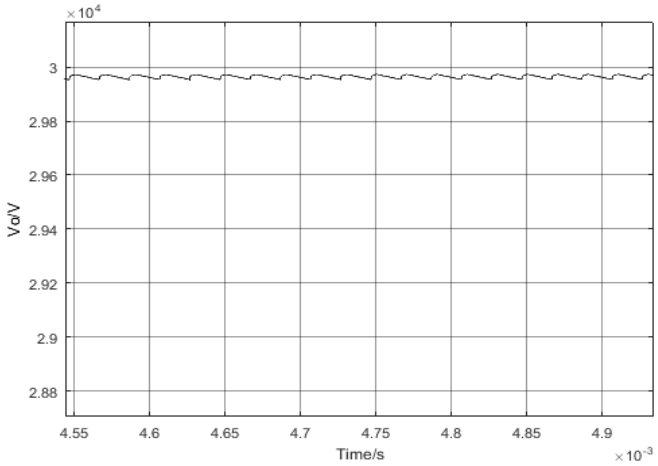

(b) C-W positive and negative bidirectional voltage doubling rectifier circuit

Fig. 4. Output ripple waveform of the two methods

3.4 Selection of main devices

3.4.1 Selection of continuous current diode

The maximum reverse voltage that the diode bears is

$$U_{DM} = \sqrt{2}U_n = \sqrt{2} \times 300 = 424.2V \tag{9}$$

where U_n is the output voltage of inverter circuit. Considering the margin of three times, the maximum withstand voltage of diode is

$$U_{TN} = 3 \times 424.2 = 1272.6\,\text{V} \tag{10}$$

In this design, 1300V is taken. The maximum current is 0.5A. Three times of the safe reserve current is taken to ensure safe operation. In conclusion, fast recovery diode ERD09-13 is selected in this design.

3.4.2 Selection of power switch tube

The choice of switching devices is vital in the inverter circuit. At present, MOSFET and IGBT are widely used. Both of them have the advantages of fast switching speed and simple driving circuit [19]. However, the on resistance of IGBT is only 10%-30% of MOSFET under the same voltage and the efficiency is higher than MOSFET. Therefore, IGBT is selected as the switching device in this paper. Since the output voltage of the inverter is 300V, considering three times of the margin, the IGBT with withstand voltage above 900V is selected and the current is 2.5A. Hence, GT8Q101 is selected as IGBT tube.

3.4.3 The selection of HV capacitor in the voltage doubling circuit

The maximum input voltage of transformer is 300V and the transformation ratio is 1:10, the input voltage of voltage doubling rectifier is 3000V. The capacitance withstand voltage is twice the input voltage of the voltage doubling rectifier circuit. After considering the margin, MLC-LS is selected as the high-voltage capacitance, the withstand voltage is 12kV and the capacity is 10uF.

4. Research of control strategy

4.1 Single neuron nonlinear adaptive PID control strategy

Since the neural network has the ability to approach the nonlinear controlled object well, the single neuron model is adopted for design. As shown in Fig. 5, the single neuron model is an artificial neuron of McCulloch-Pitts model obtained by abstracting and simplifying human brain neurons, in which neurons are the most basic control units in neural network control.

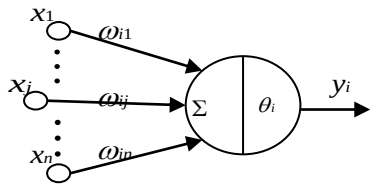

Fig. 5. Neuron model

It can be seen from Fig. 5, for the *i*th neuron, x_1, x_2, ……, x_n are the received information by the neuron, ω_1, ω_2, ……, ω_n are the connection strength, which is also known as weight. By combining the effects of input signals through linear weighted summation, the net input is obtained as follows.

$$net_i = \sum_{j=1}^{n} \omega_{ij} x_j - \theta_i \tag{11}$$

where θ_i is the threshold of neuron *i*. The output y_i of neuron *i* is the activation function of the current state, which is expressed as

$$y_i = g\left(net_i\right) \tag{12}$$

The single neuron adaptive PID control is improved and optimized on the basis of traditional PID control and combined with the advantages of simple structure and small computation of traditional PID control. The controller is formed by setting the input of a single neuron to the ratio, integration and differentiation of the difference between the expected output and the actual output. A block diagram of a single neuron adaptive PID control system is shown in Fig. 6.

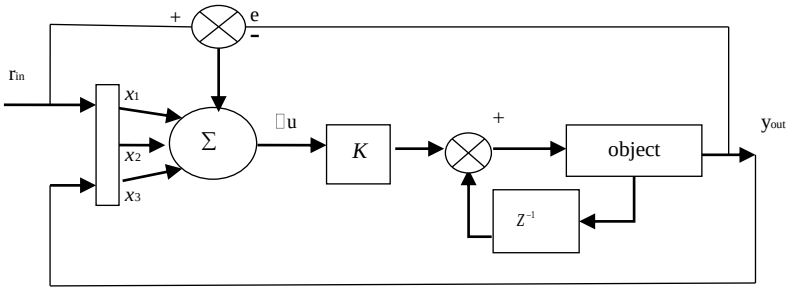

Fig. 6. Single neuron adaptive PID control structure

The single neuron adaptive controller realizes the self-adaptive and self-organizing function by adjusting the weight coefficient, and the adjustment of the weight coefficient is based on the supervised Hebb learning rule. The control algorithm and learning algorithm are as follows.

$$u(\tau)=u(\tau-1)+K\sum_{i=1}^{3}\omega_i'(\tau)x_i(\tau) \tag{13}$$

$$\omega_i'(\tau)=\omega_i(\tau)/\sum_{i=1}^{3}\left|\omega_i(\tau)\right| \tag{14}$$

$$\omega_1(\tau)=\omega_1(\tau-1)+\eta_I z(\tau)u(\tau)x_1(\tau) \tag{15}$$

$$\omega_2(\tau)=\omega_2(\tau-1)+\eta_P z(\tau)u(\tau)x_2(\tau) \tag{16}$$

$$\omega_3(\tau)=\omega_3(\tau-1)+\eta_D z(\tau)u(\tau)x_3(\tau) \tag{17}$$

$$x_1(\tau)=e(\tau) \tag{18}$$

$$x_2(\tau)=e(\tau)-e(\tau-1) \tag{19}$$

$$x_3(\tau)=\Delta^2 e(\tau)=e(\tau)-2e(\tau-1)+e(\tau-2) \tag{20}$$

$$z(\tau)=e(\tau) \tag{21}$$

where η_I, η_P and η_D are the learning rates of integral, proportional and differential respectively, and K is the proportional coefficient of neurons, $K > 0$. Different learning rates η_I, η_P and η_D are adopted for integral I, proportion P and differential D so as to adjust different weight coefficients respectively.

4.2 Single neuron adaptive PID controller model

The single neuron adaptive PID controller model is established by Simulink simulation according to the single neuron adaptive PID controller model algorithm, as shown in Fig. 7.

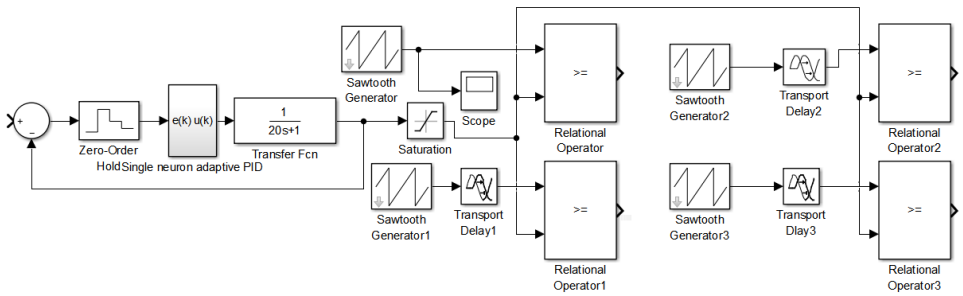

Fig. 7. Simulation model of single neuron adaptive PID controller

The transfer function of the controlled object is

$$Gs = \frac{1}{20s+1} \tag{22}$$

4.3 Parameter setting

For the setting of learning rates η_I , η_P and η_D , the smaller value can be taken first. If the process from overshoot to stabilization takes a long time, η_P and η_D can be appropriately increased, and vice versa. If the response characteristics show short rise time and excessive overshoot, η_P should be reduced; on the contrary, it increases. The setting of the weight coefficient $\omega_i(k)$ is realized by using supervised Hebb learning rules. The special rules are as follows.

(1) Select the initial value $\omega_i(0)$ of the weight coefficient $\omega_i(k)$;

(2) Calculate $x_i(k)$ from Eqs (18) ~ (20);

(3) Get the state output $\Delta u(k) = K\sum_{i=1}^{3}\omega_i(k)x_i(k) - \theta$ from Eqs (13) ~ (17);

(4) Calculate y;

(5) Adjust $\omega_i(k)$, if the actual output is consistent with the set value, $\omega_i(k)$ is stable; otherwise, return to step (2) until $\omega_i(k)$ reaches the set value.

5. Simulation and result analysis

5.1 Comparison of common signal tracking results

Two common signals step signal and sine signal are used to test the performance of the proposed method. Traditional PID controller tracking step signal and sine signal are firstly tested. In traditional PID controller simulation, K_p = 0.7, K_i = 0.03, K_D = 0.001 and sampling time is 1s. The simulation results are shown in Fig. 8 and Fig. 9.

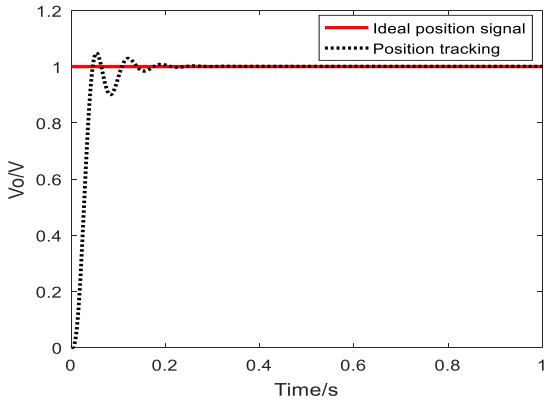

Fig. 8. Results of tracking step signal with traditional PID

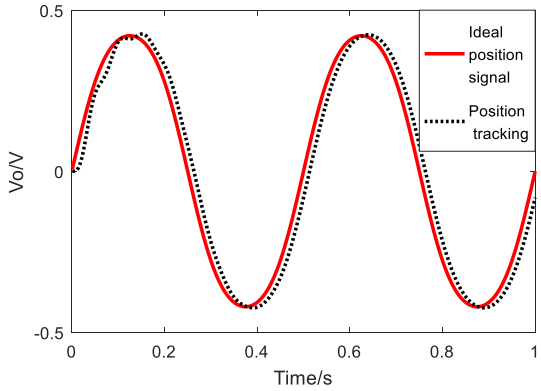

Fig. 9. Results of tracking sine signal with traditional PID

The single neuron PID controller with supervised Hebb learning rule is also used to track the step signal and sinusoidal signal. The parameters are set to $\eta_p = 50$, $\eta_i = 10$, $\eta_D = 15$, and K = 0.09 by continuous adjustment. The sampling time is 1s. The initial weight is reselected as $\omega_p = \omega_i = \omega_D = 0.1$. The system output and weight adjustment changes are shown in Fig. 10 ~ Fig. 12.

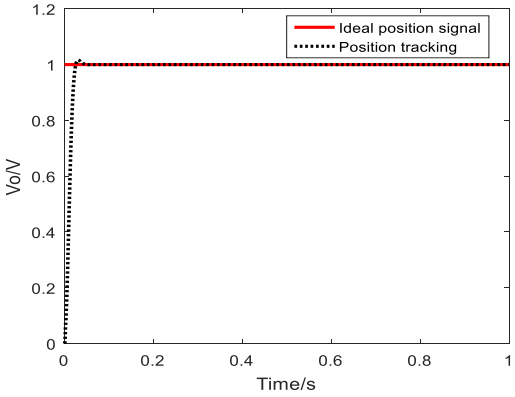

Fig. 10. Results of tracking step signal with single neuron adaptive PID control

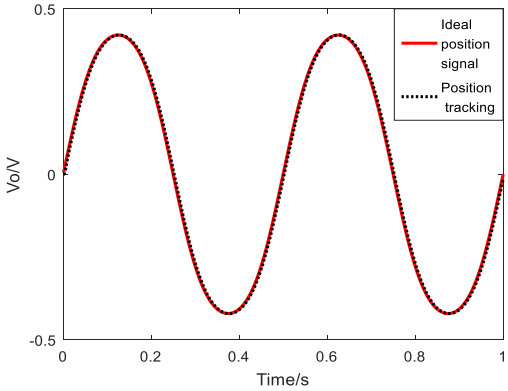

Fig. 11. Results of tracking sine signal with single neuron adaptive PID control

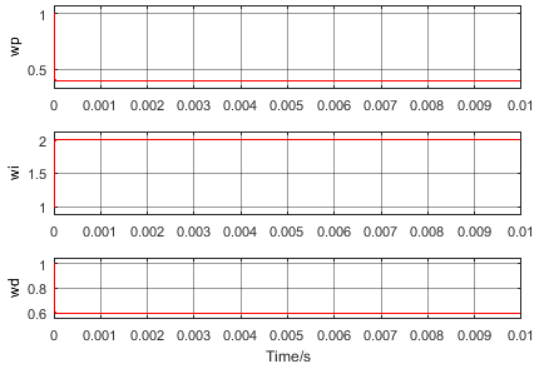

Fig. 12. Weight curve of single neuron adaptive PID control

The control effects of traditional PID control and single neuron adaptive PID control are list in Table 1 by comparing the rise time, overshoot and adjustment time.

Table 1

Performance indexes of two controllers

Two controllers	Rise time (s)	Overshoot (%)	Adjustment time (s)
Traditional PID control	0.054	4.8%	0.29
Single neuron adaptive PID control	0.028	1.6%	0.051

It can be seen from Table 1that the single neuron adaptive PID control has more excellent tracking effects than traditional PID.

5.2 Experimental test and analysis of high voltage power supply

According to the analysis and modeling of the HV power supply, the mathematical model is the controlled object of the simulation. Set the ideal output voltage V_O = 30KV, and then carry out the traditional PID and single neuron PID control respectively. The results of traditional PID control and single neuron adaptive PID control are shown in Fig. 13 and Fig. 14.

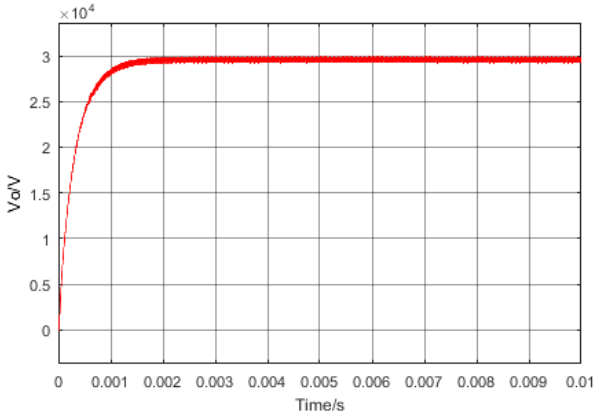

Fig. 13. Traditional PID control simulation output

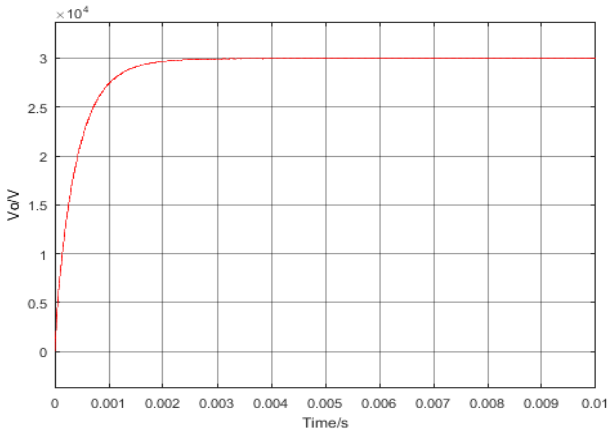

Fig. 14. Single neuron adaptive PID control simulation output

The output ripple voltage is calculated as

$$\gamma = \frac{U_{o\max} - U_{o\min}}{U_{o\max}} \times 100\% = \frac{3.04KV - 2.96KV}{3.04KV} \times 100\% = 2.6\% \tag{23}$$

The simulation results show that the single neuron adaptive PID control effects are obviously superior to the traditional PID control with low overshoot，high rise rate and good stability, which has good control effect on the nonlinear object.

6. Conclusions

In this paper, a novel HV power supply of the medical mammography X-ray machine is designed based on single neuron nonlinear adaptive PID control. The hardware part adopts soft switch technology and positive and negative two-way voltage doubling rectification, which greatly reduces the switching loss and voltage ripple. The single neuron nonlinear adaptive PID control improves the stability of the output voltage, shortens the rising time, improves response speed and enhances the robustness. In future work, the research will further increase the output voltage to several hundred thousand volts and expand the application field.

Acknowledgements

This work was supported by National Natural Science Foundation of China (61503169) and Liaoning province innovation talent project (LR2016057).

REFERENCES

[1]. *Y. Chen, K. Zhang, X. Zhao*, "Design of parameter self-tuning fuzzy PID controller for vacuum metallurgy", in Journal of Vacuum Science and Technology, **vol. 34**, no. 5, 2014, pp. 528-532.

[2]. *J. G. Huang, J. Wang, H. Fang*, "An anti-windup self-tuning fuzzy PID controller for speed control of brushless DC motor", in Automatika, **vol. 58**, no. 3, 2017, pp. 321-335.

[3]. *T. Qu, B. B. Hao*, "Single-neuron PID control arithmetic with integral restriction function", in Journal of Aerospace Power, **vol. 28**, no. 6, 2013, pp. 1415-1419.
[4]. *A. I. Bhatti, S. K. Spurgeon, X. Y. Lu*, "A nonlinear sliding mode control design approach based on neural network modeling", in International Journal of Robust & Nonlinear Control, **vol. 9**, no. 7, 2015, pp. 397-423.
[5]. *C. Yu, Z. Zhou, Z. Chen*, "Research on Neural Network Predictive Control of Induction Motor Servo System for Robot", in Advances in Intelligent Systems and Computing, **vol. 250**, 2014, pp. 147-156.
[6]. *C. Tao, J. Wan, J. Ai*, "A nonlinear control approach for a hypersonic vehicle", in Aircraft Engineering and Aerospace Technology, **vol. 89**, no. 2, 2017, pp. 320-329.
[7]. *Q. Wang, C. Y. Tang, T. S. Wang*, "Resonant pole soft-switching inverter with transformer-assisted commutation", in Electric Machines & Control, **vol. 21**, no. 11, 2017, pp. 73-81.
[8]. *Y. Chen, G. Wang, X. Su*, "Design of high voltage power converter for traveling wave tube amplifier", in Journal of Electronics, **vol. 31**, no. 6, 2014, pp. 587-596.
[9]. *N. N. Blinov, E. B. Kozlovskiĭ, O. V. Romanov*, "A New Stage for Standardization of Medical X-Ray Equipment", in Meditsinskaia tekhnika, **vol. 47**, no. 5, 2014, pp. 16-23.
[10]. *C. Dong, J. Xue, Y. Hu*, "Control Study of Pulsed MIG High-Speed Welding Power Source Based on Single Neuron Adaptive PID Model", 2018 10th International Conference on Intelligent Human-Machine Systems and Cybernetics (IHMSC), Hangzhou, 2018, pp. 381-385.
[11]. *Y. Chen, K. Zhang, X. Zhao*, "Design of parameter self-tuning fuzzy PID controller for vacuum metallurgy", in Journal of Vacuum Science and Technology, **vol. 34**, no. 5, 2014, pp. 528-532.
[12]. *A. Ioinovici*, "Power Electronics and Energy Conversion Systems, Fundamentals and Hard-switching Converters", in Journal of Electrical Technology, **vol. 28**, no. 2, 2015, pp. 155-159.
[13]. *J. Li, F. B. M. V. Horck, B. J. Daniel*, "A High-Switching-Frequency Flyback Converter in Resonant Mode", in IEEE Transactions on Power Electronics, no. 99, 2016, pp. 1-7.
[14]. *M. Uenaka, Y. Tanaka, A. Nakabayashi*, "Design Approach of Non-Isolated Converters with Passive Soft Switching", in IEEJ Transactions on Industry Applications, **vol. 137**, no. 11, 2017, pp. 837-843.
[15]. *A. A. Trubitsyn, E. Yu, Grachev*, "A High-Voltage Power Supply for a Microfocus X-Ray Tube", in Instrument and experimental technology, **vol. 62**, no. 5, 2019, pp. 640-645.
[16]. *G. Q. Gao, Q. f. Wang, Q. X. Liu*, "Energy transfer efficiency for magnetic core of linear transformer driver", in High Power Laser & Particle Beams, **vol. 22**, no. 1, 2010, pp. 211-215.
[17]. *W. C. Hsu, J. F. Chen, Y. M. Wu*, "Design and Steady State Analysis of Parallel Resonant DC-DC Converter for High Voltage Power Generator", in IEEE Transactions on Power Electronics, **vol. 32**, no. 2, 2016, pp. 1-10.
[18]. *Y. Xing, X. Zhan, T. Xia*, "High step-up isolated resonant converter with voltage quadrupler rectifier and dual-phase-shift control", in IET Power Electronics, **vol. 8**, no. 12, 2015, pp. 2462-2470.
[19]. *N. R. Bouda, J. Pritchard*, "Methods of high current magnetic field generator for transcranial magnetic stimulation application", in Journal of Applied Physics, **vol. 117**, no. 17, 2015, pp. 1171-1178.